JOURNAL OF GEOPHYSICAL RESEARCH, VOL. 104, NO. D22, PAGES 27,921-27,933, NOVEMBER 27, 1999

Land cover mapping at BOREAS using red edge spectral parameters from CASI imagery

Pablo J. Zarco-Tejada
Centre for Research in Earth and Space Science, York University, Toronto, Ontario, Canada

John R. Miller
Department of Physics and Astronomy, York University, Toronto, Canada

Abstract. Scientific and technical challenges remain to accurate classification of land cover and forest species as a result of the many spectral and spatial variables influencing surface reflectance, coupled with the constraints imposed by the spectral and spatial characteristics of the remote sensing instrumentation. The use of systematic differences in canopy pigment or chemistry by cover type or by species as a basis for land cover classification has very recently emerged as a potentially new approach. In this study classification of land cover is investigated, based on chlorophyll content variations as inferred from spectral bands in the red edge reflectance region. This analysis was carried out on data collected with the Compact Airborne Spectrographic Imager (*casi*) for a 16 km x 12 km image mosaic over the sub-modeling grid of the Southern Study Area at the BOReal Ecosystem-Atmosphere Study (BOREAS). The analysis demonstrates that land cover mapping, based solely on red edge spectral parameters, appears to be feasible, robust, and for some cover classes outperforms other current classification methods. Classification accuracy assessments of the derived land cover maps were performed using a forest inventory map provided by the Saskatchewan Environment and Resource Management Forestry Branch – Inventory Unit (SERM-FBIU). The red-edge parameter-based land cover classification showed producer's accuracies which exceeded 68.6% for all classes identified: conifers (however, without an ability to separate wet from dry conifers), mixed stands, fen and disturbed and regeneration features. The corresponding user's accuracies for these classes ranged between 58 and 66%, with the overall classification accuracies of 61.15% and Kappa coefficient (K) of 0.52. In comparison, the corresponding Kappa coefficients for the cover classification using 16 channel *casi* data and for a TM-based classification, were 0.36 and 0.29, respectively. Results of this study suggest that whereas land cover classification accuracy improvements for the important, but illusive, fen cover type in the boreal ecosystem are possible using classifications based on red edge parameters, significant uncertainties remain in the estimated aerial extent.

1. Introduction

A critical contribution of remote sensing science to BOREAS is the provision of accurate land cover information at local and regional scales for a variety of purposes [*BOREAS Experiment Plan*, 1994; *Sellers et al.* 1995]. Land cover data for the northern and southern Study Areas in BOREAS is needed along with estimation of biophysical variables such as leaf area index, biomass, and primary productivity to serve as input in the modeling of carbon exchange in the boreal forest [*Sellers and Schimel*, 1993; *Running and Gower*, 1991]. Land cover characteristics influence many of the mass and energy exchange processes at the land-atmosphere interface [*Cihlar*, 1997] with a functional dependency on the land cover type. Therefore accurate spatial distribution and percent aerial coverage of the major cover types is essential for correct process modeling in the boreal region.

At the coarse spatial resolution scale suited to the entire BOREAS region (approximately 500,000 km^2), land cover classification has been provided using multi-temporal 1992 AVHRR data [*Steyaert and Loveland*, 1995; *Steyaert et al.*, 1997] and also from a separate study using 1993 AVHRR data in combination with higher spatial resolution classifications derived from Landsat TM data [*Cihlar et al*., 1997]. Although these data sets are critical for modeling at the regional scale concerns persist about accuracy due to cover heterogeneity (e.g. fens, bogs and small lakes) relative to the effective spatial resolution of multi-temporal AVHRR [*Steyaert et al.*, 1997]. At finer resolution corresponding to the BOREAS intensive northern and southern study areas (approximately 7000 km^2 each) land cover has been mapped with Landsat TM utilizing a physically-based classification algorithm that employs geometric canopy reflectance models [*Hall et al.*, 1995; 1997]. This physically-based approach showed classification accuracies superior to those obtained with conventional statistically based-algorithms (supervised and unsupervised classification), and it was found more robust over larger areas [*Hall et al*, 1997]. This approach is thought to represent an improvement over purely statistical methods: it permits highly nonlinear multispectral class distribution functions to be characterized, classifier training is simplified since only end member reflectance values are

required (although not generally available except through field measurements), signature variations due to view/illumination angles, canopy cover and other factors are inherently accounted for, and perhaps most-importantly, it permits the direct estimation of certain canopy biophysical variables [*Hall et al*., 1997]. Nevertheless, classification accuracies remain generally low for fen (a major source of methane in the boreal region) and dry conifers. Accordingly, improvements in land cover mapping are a continued priority and the subject of currently active research for BOREAS and for global mapping. Enhancements of the physical-modeling approach [*Hall et al.*, 1997; *Peddle et al.*, 1997], neural networks [*Benediktsson et al.*, 1990; *Duguay and Peddle*, 1996], active-microwave for mapping boreal biomass [*Ranson et al.*, 1997], multi-angle and polarization signatures are examples of such efforts.

A new paradigm for the classification of land cover has recently been reported which exploits systematic differences by species of the reflectance in the short wave infrared spectral regions sensitive to foliar chemistry (Martin *et al*., 1998). Similarly in this paper, we describe classification of vegetated land cover based on spectral parameters that characterize the red edge reflectance region, which are responsive to foliar chlorophyll pigment levels. Using airborne imagery from *casi* over the BOREAS southern study area modeling grid (16 x 15 km), a land cover mapping algorithm/approach is presented based on unsupervised classification with three red edge spectral parameters: the red edge inflection point (λ_p), the wavelength at the reflectance minimum (λ_o), and a shape parameter (σ), as defined by the inverted-gaussian red-edge curve-fit model [e.g. *Hare et al.*, 1984], and discussed by *Miller et al.* [1990; 1991]. Our hypothesis is that the separation of land cover types using this classification paradigm is based on cover-type systematic differences in the variables known to affect red edge spectral parameters: vegetation chlorophyll content, canopy structure, canopy cover, and illumination.

Previous studies reported changes in the slope and position of the red edge with leaf chlorophyll [*Horler*, 1980; 1983] as healthy leaves progress from active photosynthesis through various stages of senescence due to loss of chlorophyll and the addition of tannins [*Knipling*, 1969]. Early work focused on the red edge as a measure of vegetation stress where a shift in the position of the red edge to shorter wavelengths was correlated with reductions of chlorophyll-*b* and a relative decrease of chlorophyll in mineral-stressed vegetation [*Chang and Collins*, 1983; *Collins et al*., 1981; 1983; *Horler et al*., 1980; 1983; *Milton et al*., 1983] and for needles of high-damage sites in areas of forest decline in northeast USA [*Rock et al*., 1988]. Similarly, strong red edge parameter/chlorophyll relationships have been reported for a variety of vegetation stands: sugar maple [*Vogelmann et al*., 1993], slash pine [*Curran et al.*, 1995], BOREAS conifer stands [*Dawson*, 1998], and grass [*Pinar and Curran*, 1996]. In these and other studies spectral indices demonstrated a high correlation with leaf chlorophyll-*a* and chlorophyll-*b* concentrations and total canopy chlorophyll content in particular vegetated cover types. Studies have used leaf chlorophyll concentration and/or canopy chlorophyll content as variables against which to correlate optical indices; *Matson et al.* (1994) provide a useful description of the distinction and significance between these chlorophyll measures.

If vegetated land cover is to be separated by chlorophyll content, differences in phenological cycles between cover type as well as any species-specific differences in the chlorophyll/red-edge parameter relationships would need to be exploited. Some insight is provided by the seasonal laboratory-based leaf measurement study [*Belanger et al*., 1995] of the chlorophyll/red-edge parameter relationships for 5 deciduous species in southern Ontario (Canada); important findings were: (i) the red edge spectral parameter λ_o exhibited the most significant relationship with total seasonal chlorophyll on a leaf-area basis, (ii) the tracking of the seasonal cycle of chlorophyll in the leaves of the range of tree species and certain red edge wavelength parameters suggested the potential for measuring chlorophyll content by remote sensing for canopies of different species or mixed canopies, (iii) the ability to separate species through chlorophyll content was dependent on the particular species and on the date of observation, with maximum separability generally in the early fall. Observations (i) and (ii) above are consistent with those of *Matson et al*. [1994] who found that red edge parameters from remote sensing imagery tracked seasonal variations in canopy chlorophyll across a range of conifer stands.

The issue of the sensitivity of red edge parameters to canopy structure and understory has received relatively less attention due primarily to the paucity of suitable airborne/field data. Modeling studies by *Baret et al.* [1992] using a combination of a leaf biochemical model (PROSPECT), a closed canopy model (SAIL) model and an atmospheric model (5S) suggest that LAI and to a lesser extent solar-viewing geometry are expected to have an effect. Comparable experimental work is limited, especially in open conifer canopies. *Filella et al*. [1994] have studied the red edge position as an estimator of leaf area index (LAI) and hydric status. Red edge position, amplitude of red edge peak and area of red edge peak were studied and correlated with chlorophyll content, LAI and water content. The area of the red edge peak was the best estimator of LAI, and the red edge position was highly correlated with chlorophyll content.

Mapping with spectral parameters has the inherent advantage that these are relatively insensitive to variations to illumination (e.g. *Rencz et al.* [1986] showed red edge position invariant across cloud shadow boundaries in airborne imagery) or inaccuracies in atmospheric correction

(this study, and *Baret et al.* [1992]); therefore, an algorithm based on spectral parameters offer some potential advantages over other purely statistical or reflectance-based classification algorithms. The primary disadvantage is the requirement for sensors with sufficient spectral resolution and judicious band placement on the red edge to allow land cover mapping as described here. This restricts data sources to airborne imaging spectrometer type sensors (e.g. AVIRIS (Airborne Visible/Infrared Imaging Spectrometer), *casi*) and to selected satellite sensors (e.g. MERIS on Envisat, and proposed targeting imaging spectrometers).

2. Data description

Three different data sets from the Southern Study Area - Modeling Sub-Area were used in the present study on land cover classification: (i) surface reflectance data from the *casi* collected at 3 m spatial resolution and in 16 spectral channels, which permitted the generation of images of red edge spectral parameters; (ii) forest cover data for detailed validation of land cover classes, provided by Saskatchewan Environment and Resource Management, Forestry Branch – Inventory Unit (SERM-FBIU) as derived from infrared aerial photography and field reconnaissance notes; and (iii) a classified Landsat-TM scene to provide an intercomparison of land cover products. A description of these three data sets is provided below.

2.1. Mosaicked Airborne Multispectral Image Data

The *casi* sensor, which is a push-broom imager collecting data in the visible and near infrared wavelength regions (400-950 nm), was flown August 1, 1996 over the Modeling Sub-Area of the Southern Study Area near Prince Albert, Saskatchewan as part of the BOREAS project field deployment. The *casi* operation configuration for the study site was the "Spatial Mode" in which imagery is obtained at full spatial resolution of 512 spatial pixels across the 37.5° swath, in 16 spectral bands and at 16-unsigned bits data quantization. The spectral characteristics of the data set are shown in Table 1. The altitude above ground level was 2500 m with integration time of 27 ms giving a spatial resolution of 3.1 x 2.9 m, re-sampled to 3 x 3 m in the analysis geocorrection step.

The study area of 16 x 12 km had to be acquired in multiple images collected consecutively. The acquisition of the images began at 18.37 UTC and finished at 20.49 UTC, with slowly varying sky haze conditions and some isolated cloud development. During this data acquisition period the sun's position, given as (solar zenith angle, solar azimuth angle), changed from (36.2°, 169.5°) to (38.8°, 210.2°). Each 512 pixel-wide image swath covered approximately 1536 m; in order to cover the entire area, 11 image strips were acquired with approximately 500 m overlap between consecutive images.

Table 1: Spectral characteristics of the *casi* sensor for this study

Channel	Center Wavelength (nm)	Channel Range (nm)	Start Wavelength (nm)	End Wavelength (nm)
1	411.5	7.9	403.5	419.4
2	442.2	5.1	437.0	447.4
3	468.3	5.2	463.1	473.5
4	487.0	5.2	481.8	492.2
5	530.1	5.2	524.8	535.3
6	554.5	5.2	549.2	559.7
7	644.9	5.3	639.6	650.2
8	665.7	5.3	660.4	671.0
9	677.1	5.3	671.8	682.4
10	704.6	6.3	698.3	710.9
11	747.4	5.3	742.1	752.7
12	774.1	5.3	768.8	779.5
13	858.5	5.3	853.2	863.8
14	869.1	6.3	862.8	875.4
15	904.8	5.3	899.5	910.1
16	935.8	5.3	930.4	941.1

Due to the size of the grid area, the data collection was designed to optimize the total acquisition time by flying in a race track fashion with swaths at the east side of the grid flown with a northerly heading and swaths at the west side of the image flown with a southerly heading. The resulting mosaic encompassed 3 of the flux tower sites: Fen, OJP (mature Jack Pine) and YJP (young jack pine).

The eleven images of the study site were processed to at-sensor radiance and then to at-ground reflectance. The sensor radiometric calibration, carried out in the laboratory prior to deployment, produces Radiance Sensitivity Factor (RSF) values that are applied to the *casi* imagery [*Gray et al.*, 1997], appropriate to the date of data acquisition and the lens f-stop. The at-sensor radiance is converted to at-ground reflectance using an atmospheric correction model based on a modified version of the 5S model, called CAM5S [*O'Neill et al.*, 1996]. The required input aerosol optical depth was interpolated from data collected at 7 minute intervals from a sun photometer located at the Paddockwood school; aerosol optical depth at 550 nm changed from 0.10 to 0.12 during the mission [*Markham et al.*, 1997]. The reflectance retrieval accuracies reported in validation experiments performed during similar *casi* deployments in July 1994 were 0.006 absolute error in the visible and 0.014 in the near infrared for a sampling of reference targets [*O'Neill et al.*, 1997].

The resulting composite image is shown in Plate 1 [*Zarco-Tejada*, 1998]. Some radiometric striping is discernable in the image on the east side of the modeling area (right side of the Plate). There was cumulus cloud build-up to the east of edge of the study site during the course of the 2.5 hour image acquisition period; cloud-scattering illumination effects are the most likely cause of the observed BRDF reflectance variations across the *casi* 37.5° swath, and flight-line dependent radiometric variations on the east side of the

imaged area. In addition, an occasional isolated cloud was observed below the sensor during the acquisition, as is seen in the imagery.

2.2. SERM-FBIU Forest Cover data set

A forest cover data set of the Modeling Sub-Area in the BOREAS Southern Study Area was provided by the Inventory Unit of the Saskatchewan Environment and Resource Management, Forestry Branch (SERM-FBIU). The data set was prepared by the BOREAS Science staff by processing the original vector data into raster files. The parameters provided include species association (cover type), crown closure, height class and year of stand origin or disturbance. The original data were digitized from 1:12500-scale forest cover maps derived from 1:12500-scale infrared aerial photography and field reconnaissance work. The data set provided covers a portion of the BOREAS Southern Study Area and most of the associated SSA-Modeling Sub-Area, and has been gridded to a cell size of 30 m.

The data set was produced from aerial photography taken as recently as 1988, but the data set is maintained by SERM-FBIU and updated based on fires, cutting and other disturbances. The data contain the updates made from 1988 to 1993, when the data set was acquired by BORIS (BOREAS Information System).

The species association data set covering the area had 20 different classes: white spruce, black spruce, jack pine, tamarack, spruce/pine, mix spruce-fir/broadleaf, mix jack pine/broadleaf, mix broadleaf/spruce-fir, mix broadleaf/jack pine, aspen, treed muskeg, clear muskeg, brushland, clearing, burn-over, disturbed/cut/burn, disturbed/jack pine regeneration, experimental area, flooded land and water. It is necessary to transform this baseline land cover type data to functional land cover classes deemed of interest to BOREAS science, as described in detail in *Steyaert et al.* [1997] and *Hall et al.* [1997]; the resulting 7 classes: conifer (dry), conifer (wet), mixed, deciduous, fen, disturbed/miscellaneous and water, are listed in Table 2 along with aerial fractions, and the corresponding baseline land cover map is shown in Plate 2.

2.3. Land cover classification by Landsat TM

The classified Landsat TM image of the Southern Study Area was provided by the BOREAS science staff, as a result of a physically-based classification using canopy reflectance models to account directly for signature variations from sun angle, canopy closure, etc. [*Hall et al*, 1997]. The image was acquired on September 2, 1994 and processed at the Canada Centre for Remote Sensing (CCRS). This scene is Path 37, Row 22-23 (shifted) in the *Landsat Worldwide Reference System* (WRS), with solar elevation angle at the time of image acquisition of 40.1 degrees and solar azimuth angle of 146 degrees. The imagery was converted to surface reflectance before the classification was performed. Atmospheric correction coefficients were computed using optical depths from a sun photometer as input into the 6S atmospheric correction model [*Markham et al.*, 1992].

The image area covers an area of 129 km by 86 km including areas just north of Prince Albert, Saskatchewan. The spatial resolution of the image was gridded to a cell size of 30 meters from the original nominal resolution of 28.5 meters

The image was classified by NASA Goddard Space Flight Center (GSFC) personnel using a technique described in *Hall et al.* [1995, 1997] and *Peddle et al.* [1997]. In this technique, end member reflectances of canopy, background, and shadow are used with a geometric canopy model to compute simulated pixel reflectances for increasing amounts of canopy cover. These simulated reflectances can be plotted as a continuous trajectory for each class (e.g. wet conifer, deciduous, etc.) from 0% to 100% canopy cover. The imagery pixels were classified based on their proximity to the trajectories, with the pixel being assigned to the class of the closest trajectory.

Thirteen important BOREAS Carbon/Water/Energy classes were identified and are presented in *Hall et al.* [1997] (see Table 2). An error assessment on the land cover classification was performed by the BOREAS science staff. Auxiliary sites and a few randomly selected sites were used as ground-comparison data. The location of each ground "truth" site was identified on the georeferenced image as a 3 by 3 pixel area. Each of the 9 pixels in these areas represented a test point. Many classes were not represented, so classes like "Disturbed" or "Water" were not included. The corresponding reported accuracy estimates (1-omission) for the SSA area in the available land cover classification from the BOREAS documentation were: wet conifer (71%), dry conifer (50%), mixed (53%), deciduous (89%), fen (11%), new regeneration conifers (78%), medium age regeneration conifers (44%), new regeneration deciduous (100%).

For comparison with the SERM-FBIU land cover map (Plate 2), the Landsat TM-based land cover map for the BOREAS SSA derived by *Hall et al.* [1995, 1997] is reproduced in Plate 3 for the modeling sub-area covered in this study. For more effective comparisons below, the original classification comprising 13 classes was reduced to 7 functionally-important classes identified for SERM (see Table 2) by merging the smaller "other" classes into these. The visual effect is to enhance the spatial coherence of the resulting TM classification image over the BOREAS SSA modeling area. In addition, to aid visual comparison between classifications in Plates 2 and 3, identical color assignments are used for the 7 classes.

Table 2: Cover type merging into classes to permit cross-comparisons between forest inventory cover types (SERM-FBIU), *casi* red edge classes, and BOREAS functional classes derived with TM. In each case, derived cover aerial-extent percentages are given for the sub-modeling grid of BOREAS SSA

SERM classification				***casi* RedEdge Classification**			**TM Classification**		
Class	**% Single Class**	**% Aggr.**		**Class**	**% Single Class**		**Class**	**% Single Class**	**% Aggr.**
White Spruce	0.16	24.08		Conifers	36.26		Dry Conifer	-	4.17
Jack Pine	23.92								
Black Spruce	9.92	27.53					Wet Conifers	41.34	55.7
Spruce/Pine	15.34						New Reg. Conifer	4.2	
Tamarack	2.27						Med.Age.Conif.	10.16	
Mixed Spruce Fir Broadleaf	1.29	13.24		Mixed	11.95		Mixed (Conifer & Deciduous)	-	9.42
Mixed Jack Pine Broadleaf	8.95								
Mixed Broadleaf Spruce-Fir	1.02								
Mixed Broadleaf Jack Pine	1.98								
Aspen	-	0.66		Deciduous	0		Deciduous	5.3	10.6
							New Regen Decid.	4.7	
							M.Age Reg. Decid.	0.6	
Treed Muskeg	17.15	23.02		Fen	38.3		Fen	-	10.7
Clear Muskeg	5.87								
Brushland	2.47	6.79		Disturbed	11.51		Disturbed Fire Blackened	4.44	5.88
Clearing	0.77							1.44	
Burn-over	0.1								
Disturbed - cut or burn	3.29								
Disturbed - JP Regen	0.06								
Experimental Area	0.01								
Flooded land	0.09								
Water	-	0.17		Water	0		Water	-	2.11
Other	-	4.51		Other	1.98		Other	-	1.42

3. Methods and Analysis Results

Below, the methods used to generate red edge spectral parameter maps from the *casi* image mosaic, the classification methods and results are described, followed by a comparison to land cover data previously available.

3.1 Red edge spectral parameters

The reflectance shoulder region between 670 nm and 750 nm can be characterized by four parameters, using the inverted-gaussian red-edge curve-fit model [e.g. *Hare et al.* 1984], see Figure 1. Numerical fitting procedures described by *Bonham-Carter* [1988] were coded as a number of software subroutines and incorporated into the image processing software. At-ground reflectance images can then be used to produce values of each of the red-edge parameters for each pixel in the image.

The "red-edge" parameters for the Inverted-Gaussian Model (IGM) of the reflectance curve between 670 and 780 nm are defined by *Miller et al.* (1990) as:

$$R(\lambda) = R_s - (R_s - R_o)e^{-\frac{(\lambda-\lambda_o)^2}{2\sigma^2}} \qquad [1]$$

where R_s = reflectance maximum,
R_o = reflectance minimum,
λ_o = spectral position of the reflectance minimum,
λ_p = spectral position of the inflection of the Gaussian red edge reflectance curve,
and $\sigma = \lambda_p - \lambda_o$ is the Gaussian curve width parameter.

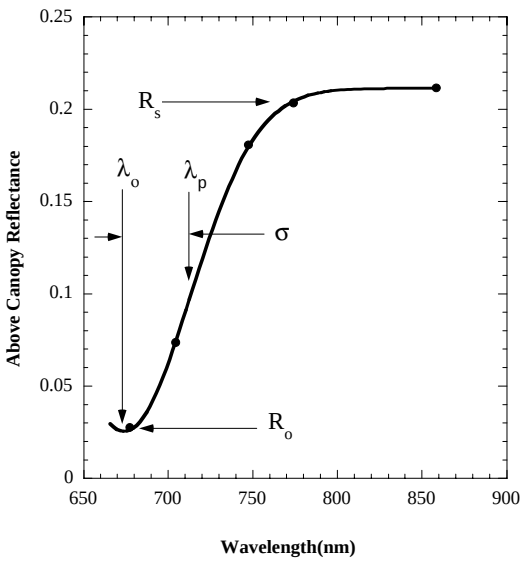

Figure 1: Inverted Gaussian Model curve fitted to a typical fen site reflectance spectrum for *casi* bands 9 to 13 (see Table 1). Reflectance red edge curve-fit parameters are indicated: the reflectance maximum (R_s), the reflectance minimum (R_o), the spectral position of the reflectance minimum (λ_o), the spectral position of the curve inflection (λ_p), and the Gaussian curve width parameter ($\sigma = \lambda_p - \lambda_o$).

That is, this curve fit defines the vegetation reflectance red-edge in terms of 2 reflectance parameters (R_s and R_o) and three spectral parameters (λ_p , λ_o , and σ), where only two are independent. Figure 1 is used to illustrate the reflectance red edge curve-fit, and the parameter definition, for a typical fen image pixel. The 16 channel *casi* reflectance imagery for this study provides four spectral bands that define the red reflectance edge (see Table 1): bands 9, 10, 11 and 12, located at 677.1, 704.6, 747.4, and 774.1 nm, respectively. The reflectance values in band 9 (677.1 nm) and band 12 (774.1 nm) provide good estimates of the reflectance parameters R_o and R_s, which then permit iterative least squares curve fitting to derive the two free spectral parameters λ_o and σ using the pixel reflectance values in band 10 (704.6 nm) and band 11 (747.4 nm). This fitting algorithm is denoted as Model 1b in *Bonham-Carter* [1988]. Thus red edge parameters can be generated on a per pixel basis for the entire image.

3.2 Spatial variability of red edge parameters

Processing involved the application of the red edge algorithm on a per-pixel basis on the 16 x 12 km *casi* image mosaic (Plate 1) after re-sampling to 30 m spatial resolution by cubic convolution; the spatial mapping of the red edge spectral parameter λ_o was produced for the study area as shown in Plate 4. Clearly there is little response to the radiometric variations observed in the source imagery (Plate 1) especially along the east side of the site. Furthermore, the variations in Plate 4 exhibit a strong spatial coherence, demonstrating robustness in the red edge reflectance curve fitting model with the *casi* imagery. Comparison to the land cover map derived from the forest inventory (Plate 2) suggests a strong association with landscape cover type. The mapping of parameter λ_o in Plate 4 using intervals of about 1 nm displays a spectral range of only 6.9 nm over the entire scene, from 671.5 to 681.8 nm. The 5 classes were generated by unsupervised classification of the λ_o parameter, specifying the number of classes as greater than five. Five major classes were generated, with a very small number of pixels out of these classes, remaining unmapped. As a consequence uneven gaps are observed between classes and the classes are of unequal spectral width.

The images of all red edge spectral parameters over the modeling grid showed evidence of spatial patterns similar to that seen for λ_o in Plate 4. Therefore an examination of the variability of the red edge parameters was undertaken across the landscape, aggregated according to landscape unit.

3.3 Land cover Classification based on Red Edge Parameters

The results generated in the study of the spatial variation in the red edge parameter λ_o across the BOREAS SSA modeling area (Plate 4), suggest that red edge spectral parameters might serve to map land cover type. A land cover mapping algorithm/approach based strictly on red edge spectral parameters has resulted from an unsupervised classification using λ_p , λ_o , and σ (Plate 5). Based on the BOREAS land cover classification in Plate 2, and the locations of the 3 flux tower sites, the five classes resulting from this image are readily identified as follows: Class 1 = mixed deciduous & conifers, Class 2 = conifers (wet and dry), Class 3 = fen (open and treed), and Class 4 & 5 = disturbed. Black areas are masked pixels arising from clouds or cloud shadows. If the hypothesis that five land cover classes are being identified is accepted then the red edge parameters can be examined within each class and mean values and standard deviations observed within each, as presented in Table 3. The basis for separation of classes is clearly seen. Red reflectance and σ progressively increase with class number, whereas λ_o, λ_p and NDVI progressively decrease.

4. Land Cover Classification Assessments

The land cover results from this study, displayed as Plates 2, 3, and 6, can be compared qualitatively by visually inspecting the spatial coherence and patterns of classes, by noting the differences in the % aerial coverage by cover class, and by doing an accuracy assessment based on the SERM data as the standard for comparison.

4.1 Derived land cover images over the modeling sub-grid

The differences between the classification results depicted in Plates 2, 3, and 6 are visually dramatic. The most important visual differences between the *casi* and the TM-based classifications are observed in the fen and in the mixed deciduous/coniferous classes which are assigned significantly larger aerial coverage and more spatial coherence by the red edge classification, apparently more representative of the SERM forest inventory results. On the other hand, a major deficit of the red edge classification is the inability to distinguish between wet and dry conifers in this August 1 image mosaic. The latter result is consistent with the small spectral differences between the red edge spectral parameters for the jack pine and black spruce tower sites (Miller and Freemantle, unpublished BOREAS results).

4.2 Classification accuracy assessments

It is possible to do a detailed classification accuracy assessment of both the *casi* red edge and the TM land cover results using the SERM-FBIU land cover type data since it is available for SSA BOREAS sub-modeling grid under study here. The BOREAS science staff have converted the original data, available from SERM-FBIU as vector polygons with attributes, into raster files. As described above, although the forest cover data layer was originally categorized in 20 land cover classes, for the purposes of this classification accuracy assessment this list was reduced to 7 classes through class merging and elimination due to small coverage: wet conifers (black spruce and tamarack), dry conifers (jack pine and white pine), mixed (coniferous & deciduous), aspen (deciduous), fen (open or treed), open water, and disturbed (see Table 2). This merging yields the “reference” land cover classification image seen in Plate 2.

With this data source selected as the standard, the approach adopted for classification accuracy assessment was to compare rasterized polygon data to classifications from the raster image data at 30 m resolution derived either from the *casi* mosaic or Landsat TM. For each class more than 60 points were selected in the middle of polygon classes (except for the water and deciduous classes which have very low aerial coverage) along with an associated 9 pixel cluster; these were compared on a pixel–by-pixel basis with the classes in the corresponding raster image pixels. The number of pixels “n” used in the accuracy assessment in each class ranged from 54 to 576 as indicated in the contingency matrix results in Tables 4 to 7. The results from this land cover classification accuracy assessment is reported for: (i) the unsupervised classification based on red edge spectral parameters (corresponding to Plate 5) (Table 4), (ii) the unsupervised classification results using the red edge spectral parameters combined with the NDVI (Table 5), (iii) the unsupervised classification using the 16 channel *casi* reflectance image mosaic (Table 6), and (iv) the land cover map based on Landsat TM (Table 7). In the accuracy assessment for a particular class, omission errors are expressed as % probability that the correct class assignment is omitted for a particular pixel; commission errors refer to % probability that a particular class is assigned to the wrong pixel. Accuracy here is interpreted in three different ways: as (i) *producer's accuracy*, 1-omission error, (ii) *user's accuracy*, which is the number of pixels correctly mapped for a particular class divided by the total number of pixels mapped as this class in the image, which includes class over-mapping due to commission errors, and (iii) overall accuracy and accuracy across all classes using the *Kappa coefficient* (K), which gives an overall accuracy assessment for the classification based on all classes commission and omission errors [Richards, 1994].

Accuracies for identified land cover classifications from red edge spectral parameters are good, ranging between 68.6% and 94.0% in producer's accuracy and 58.9% to 66.5% in user's accuracy, with overall accuracy of 61.15% and K=0.52; however, wet conifers, although an important boreal landscape component, is not separated from dry conifers. This result supports the qualitative visual similarity between the land cover images in Plates 2 and 6. In a further test, NDVI was used as an added parameter to the red edge parameters and the unsupervised classification repeated; significantly, a decrease in classification accuracies in all previously identified classes resulted (as shown in Table 5), presumably due to more significant NDVI variability within classes. Producer's accuracy ranged between 65.1% and 88.5%, with the exception of water (31.7%) which was precluded in the red edge classification methodology). User's accuracy ranged from 53.5% to 71.4%, with overall accuracy of 56.01% and K=0.46, smaller than the previous classification using the red edge spectral parameters alone. In a final test, all 16 channels of *casi* reflectance imagery were used in another unsupervised classification with the results shown in Table 6, indicating a decrease in classification accuracies in all classes, with overall accuracy of 47% and K decreasing further to 0.36.

This accuracy assessment was repeated for the TM-based land cover map in the modeling sub-area; as shown in Table 7, all classes show producer's and user's accuracies well below 50% except for wet conifers (81.1% producer's accuracy, 37.0% user's accuracy) and wet versus dry conifers remain poorly distinguished. The overall accuracy was 41.6%, and the K=0.29, low in comparison to the classification performed using red edge spectral parameters (overall accuracy=61.1% and K=0.52). Our accuracy assessment of the TM-based classification showed poorer results than those reported for the TM land cover map available from BORIS, in which only two classes were reported at below 50%. Detailed classification accuracy assessment information is included as part of the BORIS documentation on this Landsat TM land cover classification, which was based on flux tower sites (5) and auxiliary sites (~ 30) visited in the field, and regions of variability within each of these sites. However, recent but unpublished

improvements in the model-based TM classification have yet to be released but may yield accuracy improvements.

4.3 Comparison of aerial coverage of classes

Alternatively, land cover classifications can be compared by examining the % aerial extent for each of the classes over the entire sub-modeling grid; this comparison has the additional benefit of providing insight into the impact on regional flux calculations based on cover-type emission differences. The comparison between SERM and *casi* red edge results (Table 2) show that *casi* total conifers are presented at 36.26% compared to 51.61% for SERM, whereas for fen the aerial extent is 38.3% versus 23.02%; the difference is nearly the same in the two cases suggesting confusion of conifers for the fen class in *casi* results as seen in Table 4, or an erroneous simplification in equating fen with only muskeg in the SERM classification. In addition, it can be seen that the very small pure aspen class did not emerge in the red edge unsupervised classification procedure, the small pure water class was specifically excluded in the red edge analysis because of the lack of a red edge vegetation signature, and the combined disturbed/regeneration class in SERM show only 6.79% coverage compared to the *casi* red edge estimate of 11.51%. A similar comparison between the SERM aerial fractions and the TM classification reveals significant differences in most classes.

The differences between cover classification results by the aerial extent are very important for BOREAS gas flux calculations, but remain unresolved, based on this study. For example, the producer's and user's accuracies for mapping the fen with the red edge classification was 94.0% and 62.4%, respectively, while for TM-based classification the comparable accuracies are 24.9% and 50%, respectively. Yet in the comparison of the cover type aerial extent of fen percentages using the red edge classification yields 38.3% compared to TM at 10.7% and SERM at 23.02%, which is consistent with over-mapping in the *casi* red-edge classification and under-mapping in the TM classification reported in the accuracy assessment.

4.4 Effect of spatial resolution

Finally, it was considered valuable to explore the effects of spatial resolution on land cover mapping using red edge spectral parameters to examine the potential for future satellite global mapping with a sensor such as MERIS on Envisat. The *casi* reflectance image mosaic was re-sampled to 250 m (compared to a nominal MERIS resolution of 300 m) by cubic convolution and the red edge algorithm re-applied and the unsupervised classification repeated. The resulting land cover image is presented in Plate 6, using the same color key for classes to permit visual comparisons to the previous classifications. Clearly the landscape land cover patterns are generally intact at 250 m, when compared to 30 m. Perhaps of equal significance to ecosystem modeling is the effect on the inferred aerial fractions of classes; the % aerial coverage in the 16 x 12 km modeling sub-grid for 30 m compared to 250 m is: 11.95% versus 11.92% in class 1 (considered as mixed), 36.26% versus 36.67% in class 2 (dry and wet conifers), 38.3% versus 38.92% (fen) and 11.51% versus 10.74% (disturbed). This simply shows that for the boreal landscape being examined the patch size is generally larger than 250 m and similar landscape would then be amenable to land cover mapping using a red edge algorithm.

5. Conclusions

The application of a “red-edge” algorithm to *casi* mosaic image data for the BOREAS SSA modeling sub-grid has demonstrated the feasibility of the retrieval of red edge spectral parameters for the boreal landscape, in spite of imagery that showed some radiometric variability due to illumination non-uniformity from adjacent cloud build up. The landscape-scale red edge parameters revealed spatial coherence that was found to correlate well with land cover type, in spite of a range of variation of these spectral parameters of only 3 to 8 nm. Accuracy assessment of the resulting inference of land cover, when compared to forest inventory classifications, showed red edge parameter-based land cover classification accuracies which exceeded 68% for all classes identified: producer's accuracies were 81.6% for conifers (however, without an ability to separate wet from dry conifers), 68.6% for mixed stands, 94.0% for fen and 78% for disturbed. Corresponding user's accuracies were 58.9% for conifers, 66.5% for mixed stands, 62.4% for fen and 59.1% for disturbed. The overall assessments of the red edge based classification, were 61.1% (K=0.52) compared to 47% (K=0.36) and 41.6% (K=0.29) for classification with 16 channel *casi* data and for a TM-based classification, respectively. It is important to note that the accuracy assessments were performed by comparison to the vector based land cover map generated by SERM, a “*ground truth*“ with inherent errors. Therefore the comparative accuracies between classification approaches are the most important result of this study. Accuracy improvements can be expected using red edge spectral parameters as input for other classification techniques, such as supervised classification or neural networks. The unsupervised classification performed in this study using red edge spectral parameters was selected as a first approach to test the relationships between red edge and land cover types using one of the very few existent images of λ_o, λ_p and σ at high spatial resolution and covering a large spatial extent in a heterogeneous landscape. This study suggests that the aerial fraction attributed to fen in the BOREAS region has been previously underestimated, with potential implications to both gas flux modeling and hydrological modeling.

The use of reflectance parameters related to foliar chemistry (as in *Martin et al.,* 1998) or pigment content (this study) represents a new paradigm in land cover classification whose potential needs to be explored and developed. For example, if the consistency of the red edge parameters

retrievals generated in this study could be routinely observed by remote sensing in repetitive seasonal observations, subtle spectral shifts within cover classes or species might have potential significance to both land cover mapping and ecosystem functioning. Satellite mapping is limited in the near term to the MERIS sensor with its 300 m resolution in the fine mode. This study suggests that MERIS may provide an important new tool for global vegetated land cover mapping that might yield improved land cover information, especially for the fen cover class which currently poses a particular problem for successful mapping using existing optical satellite sensors.

Acknowledgments

We gratefully acknowledge the funding support from the Canada Centre for Remote Sensing, the Canadian Space Agency, the Natural Sciences and Engineering Research Council of Canada, and Macdonald, Dettwiler & Associates. We are also indebted to Jim Freemantle, Paul Shepherd, and Lawrence Gray of the Centre for Research in Earth and Space Technology for their invaluable contributions toward issues related to sensor calibrations, data acquisition, atmospheric correction and geocorrection.

References

Baret, F., S. Jacquemoud, and G. Guyot, Modeled analysis of the biophysical nature of spectral shifts and comparison with information content of broad bands, *Remote Sens. Environ.* 41, 133-142, 1992.

Benediktson, J. A., P. H. Swain, and O.K. Ersoy, Neural network approaches versus statistical methods in classification of multi source remote sensing data, *IEEE Trans. Geosci. and Remote Sens.*, 28 , 540- 552, 1990.

Belanger, M. J., J. R. Miller, and M. G. Boyer, Comparative relationships between some red edge parameters and seasonal leaf chlorophyll concentrations, *Can. J. Remote Sens.*, 21, 16-21, 1995.

Bonham-Carter, G. F., Numerical procedures and computer program for fitting an inverted Gaussian Model to vegetation reflectance data, *Comp. and Geosci.*, 14, 339-356, 1988.

BOREAS, Boreal Ecosystem Atmosphere Study Experiment Plan Version 3.0, P.J. Sellers *et al*. (eds.), NASA Goddard Space Flight Center, Greenbelt, MD, 4 volumes, 1994.

Chang, S. H., and W. Collins, Confirmation of the airborne biogeophysical mineral exploration technique using laboratory methods, *Econ. Geol.*, 78, 723-736, 1983.

Cihlar, J., J. Beaubien, Q. Xiao, J. Chen and Z. Li, Land cover of the BOREAS region from AVHRR and Landsat data, *Can. J. Remote Sens.*, 23, 163-175, 1997.

Collins, W., S. H. Chang, and J. T. Kus, Detection of hidden mineral deposits by airborne spectral analysis of forest canopies, Report NASA Contract NSG-5222, 61 pp., 1981.

Collins, W., S. H. Chang, G. Raines, F. Canney, and R. Ashley, Airborne geophysical mapping of hidden mineral deposits, *Econ. Geol.*, 78, 737-749, 1983.

Curran P. J., J. L. Dungan, and H. L. Gholtz, Exploring the relationship between reflectance red edge and chlorophyll content in slash pine II, *Tree Physiology*, 15, 203-206, 1995.

Dawson, T. P., Estimating the foliar biochemical content of forest canopies using physical models and AVIRIS spectra, *Proceedings of the First International Conference on Geospatial Information in Agriculture and Forestry*, Vol. 1, pp. 433-440, 1998.

Duguay, C. R., and D. R. Peddle, Comparison of evidential reasoning and neural network approaches in a multi-source classification of Alpine Tundra Vegetation, *Can. J. Remote Sens.*, 22, 433-440, 1996.

Filella, I., and J. Peñuelas, The red edge position and shapes as indicators of plant chlorophyll content, biomass and hydric status. *Int. J. of Remote Sens.*, 15, 1459-1470, 1994.

Gray, L., J. Freemantle, P. Shepherd, J. R. Miller, J. Harron, and C. Hersom, Characterization and Calibration of the *casi* Airborne Imaging Spectrometer for BOREAS, *Can. J. Remote Sens.*, 23, 188-195, 1997.

Hall, F. G., Y. E. Shimabukuro, and K. F. Huemmrich, Remote sensing of forest biophysical structure using mixture decomposition and geometric reflectance models, *Ecological Applications*, 5 , 993-1013, 1995.

Hall, F. G., D. E. Knapp, and F. Huemmrich, Physically based classification and satellite mapping of biophysical characteristics in the southern boreal forest, *J. Geophys. Res.*, 102, D24, 29567-29580, 1997.

Hare, E. W., J. R. Miller, and G. R. Edwards, Studies of the vegetation red reflectance edge in geobotanical remote sensing, in *Proceedings of the 9th Canadian Symposium on Remote Sensing*, pp. 433-440, Can. Remote Sens. Soc., Can. Aeronaut. and Space Inst., Ottawa, 1984.

Horler, D. N. H., J. Barber, and A. R. Barringer, Effects of heavy metals on the absorbance and reflectance spectra of plants, *Int. J. Remote Sens.*, 1, 121-136, 1980.

Horler, D. N. H., M. Dockray, and J. Barber, The red edge of plant leaf reflectance, *Int. J. Remote Sens.*, 4, 273-288, 1983.

Knipling, E. B., Leaf reflectance and image formation on color infrared film, in *Remote Sensing in Ecology*, edited by P. L. Johnson, pp. 17-29, Univ. of Georgia Press, 1969.

Markham, B. L., R. N. Halthorne, and S. J. Goetz, Surface reflectance retrieval from satellite and aircraft sensors: Results of sensor and algorithm comparisons during FIFE. *FIFE special issue, American Geophysical Union*, 18785-18795, 1992.

Markham, B. L., J. S. Schafer, B. N. Holben, and R.N. Halthore, Atmospheric aerosol and water vapor characteristics over north central Canada during BOREAS, *J. Geophys. Res.*, 102, D24, 29737-29745, 1997.

Martin, M. E., S. D. Newman, J. D. Aber, and R. G. Congalton, Determining forest species composition using high spectral resolution remote sensing data, *Remote Sens. Environ*, 65, 249-254, 1998.

Matson, P., L. Johnson, C. Billow, J. Miller, and R. Pu, Seasonal patterns and remote spectral estimation of canopy chemistry across the Oregon transect, *Ecological Applications*, 4, 280-298, 1994.

Miller, J. R., E. W. Hare, and J. Wu, Quantitative characterization of the vegetation red edge reflectance I. An inverted-Gaussian reflectance model, *Int. J. Remote Sens.*, 11, 121-127, 1990.

Miller, J. R., J. Wu, M. G. Boyer, M. J. Belanger, and E.W. Hare, Seasonal patterns in leaf reflectance red edge characteristics, *Int. J. Remote Sens.*, 12, 1509-1524, 1991.

Milton, N.M., W. Collins, S. H. Chang, and R. G. Schmidt, Remote detection of metal anomalies on Pilot Mountain, Randolph County, North Carolina, *Econ. Geol.*, 78, 605-617, 1983.

O'Neill, N. T., A. Royer, and M. N. Nguyen, Scientific and Technical Report on the Development of a Modified Version of the H5S code which incorporates major features of the 6S Code, *CARTEL internal report CARTEL – 1996-020*, 62 pp., Sherbrooke, Quebec, 1996.

O'Neill, N. T., F. Zagolski, M. Bergeron, A. Royer, J. R. Miller, and J. Freemantle, Atmospheric correction validation of *casi* images acquired over the BOREAS Southern Study Area, *Can. J. Remote Sens.*, 23, 143-162, 1997.

Peddle, D. R., F. G. Hall, E. F. LeDrew, and D. E. Knapp, Classification of forest land cover in BOREAS. II: Comparison of results from a sub-pixel scale physical modeling approach and a training based method, *Can. J. Remote Sens.*, 23, 131-142, 1997.

Pinar, A., and P. J. Curran, Grass chlorophyll and the reflectance red edge, *Int. J. Remote Sens.*, 17, 351-357, 1996.

Ranson, K. J., G. Sun, R. H. Lang, N. S. Chauhan, R. J. Cacciola, and O. Kilic, Mapping of boreal forest biomass from spaceborne synthetic aperture radar, *J. Geophys. Res.*, 102, D24, 29599-29610, 1997.

Rencz, A. N., G. F. Bonham-Carter, C. van der Greint, J.R. Miller and E.W. Hare, Preliminary results from modeling vegetation spectra derived from MEIS data, in *Proceedings of the 10th Canadian Symposium on Remote Sensing*, pp. 909 – 917, Can. Remote Sens. Soc., Can. Aeronaut. and Space Inst., Ottawa, 1986.

Richards, J. A., *Remote Sensing Digital Image Analysis. An Introduction*, Second Edition, Springer-Verlag, Germany, 1994.

Rock, B.N., T. Hoshizaki, and J.R. Miller, Comparison of in situ and airborne spectral measurements of the blue shift associated with forest decline. *Remote Sens. Environ*. 24, 109-127, 1988.

Running, S.W., and S.T. Gower, Forest-BGC, a general model of forest ecosystem processes for regional applications. II. Dynamic carbon allocation and nitrogen budgets, *Tree Physiology*, 9, 147-160, 1991.

Sellers, P. J., and D. Schimel, Remote sensing of the land biosphere and biogeochemistry in the EOS era: science priorities, methods and implementation, *Global and Planetary Change*, 7, 279-297, 1993.

Sellers, P. J., *et al*., The Boreal Ecosystem-Atmosphere Study (BOREAS): An Overview and Early Results from the 1994 Field Year. *Bull. Am. Meteorol. Soc.*, 76, 1549-1577, 1995.

Steyaert, L., and T. Loveland, 1-km AVHRR seasonal land cover classification for the Boreal Ecosystem-Atmosphere Study (BOREAS), *BOREAS Information System*, NASA Goddard Space Flight Centre, Greenbelt, MD, 1995.

Steyaert, L. T., F. G. Hall, and T. R. Loveland, Land cover mapping, fire regeneration, and scaling studies in the Canadian boreal forest with 1-km AVHRR and Landsat TM data, *J. Geophys. Res.*, 102, D24, 29581-29598, 1997.

Vogelmann, J. E., B. N. Rock, and D .M. Moss, Red edge spectral measurements from sugar maple leaves, *Int. J. Remote Sens.*, 14, 1563-1575, 1993.

Zarco-Tejada, P. J., Correlations between CO_2 fluxes and high spatial resolution reflectance imagery, M. Sc. thesis, University of Dundee, Scotland, UK, 1998.

J.R. Miller, Department of Physics and Astronomy, York University, 4700 Keele Street, Toronto, Canada M3J 1P3 (jrmiller@yorku.ca)

P.J. Zarco-Tejada, Centre for Research in Earth and Space Science, York University, 4700 Keele Street, Toronto, Canada M3J 1P3 (pzarco@yorku.ca)

(Received July 28, 1998; revised February 16, 1999; accepted February 23, 1999.)

Table 3: Mean values (± standard deviation) of red edge parameters within classes [unsupervised classification - see Plate 5] for the BOREAS SSA sub-modeling grid on August 1, 1996.

Red Edge Parameter	Class 1 (Mixed)	Class 2 (Conifers)	Class 3 (Fen)	Class 4 (Disturbed I)	Class 5 (Disturbed II)
Rs (%)	22.5 ± 9.2	17.8 ± 5.8	18.4 ± 5.0	18.6 ± 4.9	17.6 ± 5.9
Ro (%)	1.4 ± 0.5	1.8 ± 0.7	2.3 ± 0.8	4.7 ± 1.7	6.0 ± 2.1
σ (nm)	35.2 ± 0.6	35.7 ± 0.6	35.9 ± 0.6	37.7 ± 0.7	39.9 ± 0.7
λo (nm)	679.3 ± 4.4	677.6 ± 2.7	675.8 ± 0.6	674.4 ± 0.8	672.2 ± 1.0
λp (nm)	714.5 ± 0.9	712.4 ± 2.9	711.8 ± 0.7	712.1 ± 1.0	711.4 ± 1.3
NDVI	0.87 ± .04	0.81 ± .05	0.78 ± .05	0.60 ± .06	0.50 ± .04

Table 4: Land Cover Classification Assessment: Isodata unsupervised classified image using red edge λ_o, λ_p and σ parameters from *casi* image mosaic.

Unsupervised Classification		Contingency Matrix: SERM-FBIU Classification								User's Accuracy (%)
CLASS		**C1**	**C2**	**C3**	**C4**	**C5**	**C6**	**C7**	**TOTAL**	
Wet Conifers	**C1**	**470**	209	58	3	23	7	28	798	58.9
Dry Conifers	**C2**	0	**0**	0	0	0	0	0	0	0.0
Mixed	**C3**	54	37	**284**	36	0	0	16	427	66.5
Deciduous	**C4**	0	0	0	**0**	0	0	0	0	0.0
Fen	**C5**	50	121	26	2	**457**	5	71	732	62.4
Water	**C6**	0	0	0	0	0	**0**	0	0	0.0
Disturbed	**C7**	2	164	46	13	6	51	**407**	689	59.1
TOTAL		576	531	414	54	486	63	522	**2646**	
Producer's Accuracy (%)		81.6	0.0	68.6	0.0	94.0	0.0	78.0	**Overall Accuracy = 61.15%** **Kappa K = 0.52**	

Table 5: Land Cover Classification Assessment: Isodata unsupervised classified image using red edge spectral parameters λ_o, λ_p, σ, and NDVI.

Unsupervised Classification		Contingency Matrix: SERM-FBIU Classification								User's Accuracy (%)
CLASS		**C1**	**C2**	**C3**	**C4**	**C5**	**C6**	**C7**	**TOTAL**	
Wet Conifers	**C1**	**403**	179	50	2	52	5	34	725	55.6
Dry Conifers	**C2**	0	**0**	0	0	0	0	0	0	0.0
Mixed	**C3**	98	42	**289**	36	0	0	16	481	60.1
Deciduous	**C4**	0	0	0	**0**	0	0	0	0	0.0
Fen	**C5**	37	145	31	1	**430**	5	128	777	55.3
Water	**C6**	0	4	0	0	0	**20**	4	28	71.4
Disturbed	**C7**	38	161	44	15	4	33	**340**	635	53.5
TOTAL		576	531	414	54	486	63	522	**2646**	
Producer's Accuracy (%)		70.0	0.0	69.8	0.0	88.5	31.7	65.1	**Overall Accuracy = 56.01%** **Kappa K = 0.46**	

Table 6: Land Cover Classification Assessment: Isodata unsupervised classified *casi* image using 16 reflectance channels.

Unsupervised Classification		Contingency Matrix: SERM-FBIU Classification								User's Accuracy (%)
CLASS		**C1**	**C2**	**C3**	**C4**	**C5**	**C6**	**C7**	**TOTAL**	
Wet Conifers	**C1**	**327**	278	29	4	43	1	21	703	46.5
Dry Conifers	**C2**	0	**0**	0	0	0	0	0	0	0.0
Mixed	**C3**	2	2	**156**	16	0	0	6	182	85.7
Deciduous	**C4**	24	13	63	**18**	71	0	46	235	7.7
Fen	**C5**	213	200	120	4	**361**	1	123	1022	35.3
Water	**C6**	9	0	7	1	11	**59**	1	88	67.0
Disturbed	**C7**	1	38	39	11	0	2	**325**	416	78.1
TOTAL		576	531	414	54	486	63	522	**2646**	
Producer's Accuracy (%)		56.8	0.0	37.7	33.3	74.3	93.7	62.3	**Overall Accuracy = 47.09%** **Kappa K = 0.36**	

Table 7: Land Cover Classification Assessment: Classified Landsat-TM image.

Unsupervised Classification		Contingency Matrix: SERM-FBIU Classification								User's Accuracy (%)
CLASS		**C1**	**C2**	**C3**	**C4**	**C5**	**C6**	**C7**	**TOTAL**	
Wet Conifers	**C1**	**467**	282	159	12	227	23	90	1260	37.0
Dry Conifers	**C2**	12	**83**	10	1	7	5	9	127	65.3
Mixed	**C3**	57	32	**95**	20	23	4	6	237	40.1
Deciduous	**C4**	18	24	123	**21**	73	5	101	365	5.7
Fen	**C5**	12	87	11	0	**121**	3	8	242	50.0
Water	**C6**	5	18	2	0	11	**21**	14	71	29.6
Disturbed	**C7**	5	5	14	0	24	2	**294**	344	85.4
TOTAL		576	531	414	54	486	63	522	**2646**	
Producer's Accuracy (%)		81.1	15.6	22.9	38.9	24.9	33.3	56.3	**Overall Accuracy = 41.65%** **Kappa K = 0.29**	